Tunable many-body effects in triple quantum dots

Jihan Kim,[1,2] Dmitriy V. Melnikov,[1] and Jean-Pierre Leburton[1,2,3]
[1]*Beckman Institute for Advanced Science and Technology, University of Illinois at Urbana-Champaign, 405 N. Mathews Avenue, Urbana, Illinois 61801, USA*
[2]*Department of Electrical and Computer Engineering, University of Illinois at Urbana-Champaign, 405 N. Mathews Avenue, Urbana, Illinois 61801, USA*
[3]*Department of Physics, University of Illinois at Urbana-Champaign, 405 N. Mathews Avenue, Urbana, Illinois 61801, USA*
(Received 4 December 2008; revised manuscript received 26 May 2009; published 6 July 2009)

Exchange energies and charge densities for a few electrons in electrically tunable triangular and collinear triple quantum dot (TQD) systems are investigated by using the variational Monte Carlo method in the presence of magnetic fields. For $N=2$ electrons we observe a discontinuity in the J derivative with detuning voltage (dJ/dV_T) in triangular triple QDs at $B=0$ T as crossing of the eigenenergy levels leads to abrupt spatial symmetry change in the singlet and the triplet densities (density rotation) and relocalization. For $B \neq 0$ T, the angular momentum provided to the electrons quenches this effect. The density rotation is absent in the collinear TQD for all magnetic fields as the lowest excited state remains the p_x state and as such, no change in symmetry is possible. By varying the triangular TQD configuration, we show the discontinuity in dJ/dV_T persists for the top angle comprised between ~20° and ~70°. For three electrons in the symmetric triangular TQD, the monotonicity of the quadruplet-doublet energy difference from $B=0$ to 4 T remains intact for decoupled QDs but not for coupled QDs. Finally, addition energy for the triangular TQD system is computed for up to $N=3$ electrons.

DOI: 10.1103/PhysRevB.80.045305 PACS number(s): 73.21.−b, 72.20.My, 73.40.Gk

I. INTRODUCTION

In the last decade there has been extensive experimental work on man-made semiconductor quantum dots (QD).[1,2] Existence of shell structure, demonstration of Hund's rule, and the ability to control the number of electrons in both the single and the double QDs have prompted proposals on building various devices based on electron spins and charge states.[3] As an example, electron spins in QDs can be used as quantum bits (qubits), which are the basic unit of information for quantum information processing.[4] Hence, the entanglement between the spins of two electrons can be quantified by the value of exchange energy J, which is the energy difference between the lowest triplet ($S=1$) and the singlet ($S=0$) states.[5] Recently, the coherent manipulation of the two-electron spin state in coupled quantum dots has been demonstrated, which is an important milestone toward the realization of a quantum gate with solid-state systems.[6]

As the natural conceptual extension of single and double QDs, the triple quantum dot (TQD) presents a fundamental interest as an artificial triatomic molecule, where the interplay between geometrical-confinement, interdot-coupling, and many-body effects offers a rich variety of phenomena. The addition of the third dot is a logical step toward building a scalable multiqubit system used for quantum computing.[7] In the past, various devices utilizing the TQD structure have been proposed (e.g., solid-state entangler,[8] TQD charging rectifier,[9,10] and devices based on quantum cellular automat processes[11]). In this context, the electronic properties and the stability diagrams of collinear TQDs with a few electrons have been investigated experimentally[12] and theoretically with the density functional theory (DFT).[7] Recently, spin configuration in triangular TQDs with up to six electrons have been obtained and interpreted by using the Hubbard model.[13]

In this work we investigate theoretically the variations in the exchange energy between two and three electrons in TQDs by biasing one of the dot with respect to the other two QDs in the presence of magnetic fields. We use variational Monte Carlo methods (VMC) with s and p orbitals of the Fock-Darwin states as trial wave functions, which have been shown to be reliable to calculate many-body effects in coupled QDs.[14] We specifically show that the exchange interaction between the electrons can be nonmonotonically manipulated by QD detuning. In particular, for $N=2$ electrons the difference between the relocalization of the singlet- and triplet-electron densities in the QDs induced by detuning manifests as a "cusp" in the exchange energy, due to a symmetry change between the p_x and p_y single-particle states with little sensitivity to the detuned QD size. We also show that the presence of magnetic fields quenches this effect by mixing the p_x and p_y states. The abrupt variation in the exchange energy in TQDs and its dependence on magnetic fields is novel for artificial systems and, as such, it is of central importance for the manipulation of spin qubits in coupled QDs as quantum gates for quantum information processing.[2]

For $N=3$ electrons, the ground state at zero magnetic field is always the $S=1/2$ (frustrated antiferromagnetic state) state and the excited state $S=3/2$ (spin-polarized state).[13] For a simple TQD with one electron per dot, the Heisenberg Hamiltonian is described by three exchange constants

$$H^S = J_{12}\frac{1}{4}\vec{\sigma}_1\vec{\sigma}_2 + J_{13}\frac{1}{4}\vec{\sigma}_1\vec{\sigma}_3 + J_{23}\frac{1}{4}\vec{\sigma}_2\vec{\sigma}_3, \quad (1)$$

where σ is the Pauli matrix and J_{ij} is the exchange coupling constants.[15] For purposes of quantum computing, the exchange coupling J can be manipulated by each of the J_{ij}

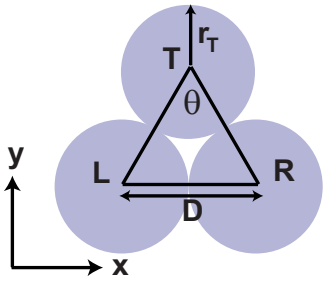

FIG. 1. (Color online) Two-dimensional schematic of the triangular TQD structure. T, L, and R denotes the top, left, and the right QDs. The separation between the dots is $D=50$ nm. r_T is the extension of the Gaussian potential from the centers of the dots.

coupling constants. In symmetric TQDs, each of the exchange coupling constants are equal to one another ($J=J_{12}=J_{13}=J_{23}$) and as a result, the exchange can be derived from the gap between the doublet ($S=1/2$) and the quadruplet ($S=3/2$) states, i.e., $\Delta_{QD}=E_{(S=3/2)}-E_{(S=1/2)}=3J/2$. In asymmetric TQDs such as in the detuning of the top QD (Fig. 10), one cannot assume the exchange coupling constants are equal since $J_{12}=J_{13}\neq J_{23}$.

The paper is divided into five different sections. In Sec. II, we describe the TQD structure and in Sec. III, the computational approach used to solve the many-body Schrödinger Equation. In Sec. IV, we provide results of our simulations for the TQD structure and analyze the effect of adding deformation, applying an external magnetic field, and changing the relative positions of the QDs. Finally, in Sec. V, we summarize the important issues mentioned in the paper.

II. TQD STRUCTURE: MODEL POTENTIAL

A schematic of a triangular TQD is shown in Fig. 1, which we model with the two-dimensional (2D) external potential

$$V_{ext}(x,y) = -V_L e^{-[(x+d_x/2)^2+(y+d_{yL})^2]/r_L^2} - V_T e^{-[x^2+(y-d_{yT})^2]/r_T^2} - V_R e^{-[(x-d_x/2)^2+(y+d_{yR})^2]/r_R^2}, \quad (2)$$

where $(-d_x/2,-d_{yL})$, $(0,d_{yT})$, and $(d_x/2,-d_{yR})$ are the respective locations of the potential minima of the left, the top, and the right dots. V_L, V_T, and V_R determine the potential depths of the QDs and r_L, r_T, and r_R specify the extensions of the Gaussian potentials from the centers of the dots. The interdot separation between the top and the other two dots is set at $D=50$ nm in all of our simulations for $N=2$ electrons. For $N=3$ electrons, the distance is varied from $D=30$ to 60 nm. Initially we set $d_x=50$ nm, $d_{yL}=d_{yR}=d_x/\sqrt{3}$, and $d_{yT}=2d_{yL}$, making the size of the three QDs equal and the triangle formed by connecting the coordinates of the three potential minima equilateral. We fix $V_L=V_R=25$ meV and vary V_T from 0 to 40 meV to detune the top QD from the two lower ones. We keep r_L and r_R constant and also vary r_T to break the symmetry among the three QDs.

III. VARIATIONAL MONTE CARLO TECHNIQUE

The model Hamiltonian for N conduction-band electrons confined in the TQDs can be written as follows:

$$H = \sum_{j=1}^{N} \left\{ \frac{\left(-i\hbar\vec{\nabla}_j - \frac{e}{c}\vec{A}_j\right)^2}{2m^*} + V_{ext}(\vec{r}_j) \right\} + \sum_{j<k}^{N} \frac{e^2}{\varepsilon|\vec{r}_j - \vec{r}_k|}, \quad (3)$$

where we use the effective-mass approximation to describe the motion among electrons in the xy plane and neglect the extension of the wave function along the z direction in a first approximation.[16] Here the external 2D potential, V_{ext}, is given by Eq. (2) and the last term of Eq. (3) describes the Coulomb interaction among electrons. We assume the material system is GaAs for which the conduction-band effective mass is $m^*=0.067m_0$, with m_0 being the free-electron mass, and the dielectric constant $\varepsilon=12.7\varepsilon_0$. $\vec{A}$ is the vector potential experienced by each electron, which is expressed as

$$\vec{A} = \frac{B}{2}(y,-x) \quad (4)$$

in the 2D symmetric gauge, where B is the magnetic field oriented along the z direction. $\vec{r}_j$ denotes the coordinates of the jth electron. We use VMC to obtain for the singlet and the triplet energies[17,18] extending previous works on single and double QDs.[14,19] The validity of our variational Monte Carlo method was shown previously upon calculating the two-electron exchange energy, J, in a model double QD potential comprised of two Gaussian functions.[14] In the double QD case, the J values agreed very well (within few μeV) with the results obtained from the exact diagonalization method for all magnetic fields ($B<6$ T). For the TQD simulations, we again use a trial wave function that has a Slater-Jastrow form, which is a product of Slater determinants consisting of single-particle orbitals for spin-up and spin-down electrons ($D^{\uparrow}$ and $D^{\downarrow}$, respectively) combined with a Jastrow term $\mathfrak{J}(r_{ij})$ to account for electron correlations

$$\Psi_T = D^{\uparrow}D^{\downarrow}\prod_{i<j}^{N}\mathfrak{J}(r_{ij}), \quad (5)$$

where $r_{ij}=|\vec{r}_i-\vec{r}_j|$.

In our simulations, we set the two-body Jastrow term to be $\mathfrak{J}(r_{ij})=e^{a_1 r_{ij}/1+b_1 r_{ij}}$ where a_1 is fixed by the cusp condition to be 0.5 for singlet and 0.25 for triplet and neglect three-body and higher correlation terms in the Jastrow term. For the single-particle orbitals located inside the Slater determinants, we use the two lowest states of circular single-dot eigenstates (Fock-Darwin states) localized in individual quantum dots,[20] given by the following expressions for the s orbitals

$$\varphi_j(x,y) = e^{-\alpha_x^2(x+d_{xs,j})^2/2}e^{-\alpha_y^2(y+d_{ys,j})^2/2}e^{-i\alpha_{bx,j}x_k}e^{-i\alpha_{by,j}y_k} \quad j=1,2,3 \quad (6)$$

and for the p orbitals

$$\varphi_j(x,y) = [(x_k+d_{xp,j})+i(y_k+d_{yp,j})]e^{-\alpha_x^2(x+d_{xs,j})^2/2} \times e^{-\alpha_y^2(y+d_{ys,j})^2/2}e^{-i\alpha_{bx,j}x_k}e^{-i\alpha_{by,j}y_k} \quad j=4,5,6,7,8,9 \quad (7)$$

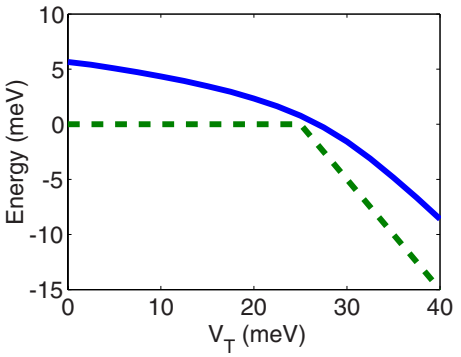

FIG. 2. (Color online) Ground-state energy as a function of the top-dot detuning in the triangular TQD structure. The dotted line indicates the bottom of the TQD system potential.

where α_x, α_y, d_{xs}, d_{ys}, d_{xp}, d_{yp}, α_{bx}, and α_{by} are treated as variational parameters. We ignore Zeeman splitting in the current analysis as it only introduces a small constant shift (~ 25 μeV/T) in the exchange energy for each magnetic field. To numerically optimize the expectation value of the energy, we use the steepest descent method in which variational parameters α_k are updated as $\alpha_k \rightarrow \alpha_k + \Delta t f_k$ at each iteration[14] where f_k is the partial derivative of energy with respect to α_k. Δt is chosen such that after an adequate number of changes in the sign of f_k, it becomes inversely proportional to the total number of iterations, allowing the variational parameters to converge numerically. By using a sufficiently large number of random walkers N_w (~ 10 millions), we solve for the expectation values of observables by utilizing the Metropolis algorithm. Upon running the numerical simulation repeatedly by using different random seeds, all final results differ by less than 20 μeV from one another.

IV. RESULTS

Figure 2 displays the single-particle ground state of the symmetric triangular TQD system ($D=50$ nm) as a function of V_T that controls the depth of the top dot. The bottom of the TQD potential is indicated by the dotted line and at $V_T=0$ meV, $V_L=V_R=25$ meV, the ground state is located at 5.65 meV. By approximating the Gaussian potential of each dot by a parabola, the confinement energy is around 8 meV, which is above the energy barrier separating the double dots and explains the lower ground-state energy. For larger values of V_T, the ground state increases above the bottom of the top dot as confinement increases with bias.

Figure 3(a) illustrates the evolution of the singlet-electron (triplet-electron) densities in a symmetric triangular TQD ($r_L=r_R=r_T=30$ nm) in the first column (second column) as V_T is varied. We keep other external parameters of the model potential constant. For $V_T < V_L=V_R$ [Fig. 3(a), row(i)], the electrons predominantly localize in the left and the right dots. As expected, the overlap between the electrons is greater for the singlet than the triplet electrons due to the Pauli exclusion principle. For $V_T=V_L=V_R$ [Fig. 3(a), row(ii)], the singlet and the triplet electron density is spread evenly over all three dots (at this point, due to the potential symmetry, the triplet is actually a linear combination of s and

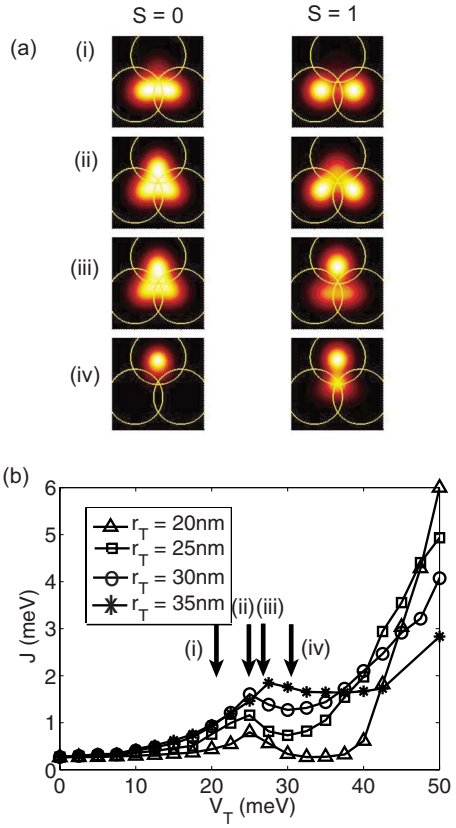

FIG. 3. (Color online) (a) Two-dimensional density plots for $r_T=30$ nm. The singlet (triplet) densities are plotted in the first (second) column under $S=0$ ($S=1$). White (dark) represents high-density (low-density) values. The circles indicate the location of the three dots. Rows (i), (ii), (iii), and (iv) correspond to $V_T=20$, 25, 25.625, and 30 meV, respectively. (b) Exchange energy J as a function of V_T for $r_T=20$, 25, 30, and 35 nm at zero magnetic field. V_L and V_R are fixed at 25 meV and $r_L=r_R=30$ nm. The arrows correspond to the density plots in Fig. 3(a) at four V_T values.

p orbitals with left-top and right-top occupations). For V_T slightly larger than $V_L=V_R$ [Fig. 3(a), row(iii)], the singlet state made essentially of s states has moved slightly to the top dot. However, the triplet state is now mostly and suddenly located in the top dot, aligned along the y direction picking up p_y-orbital components (i.e., the p_y single-particle state has dropped below the p_x state). This abrupt triplet transition is reminiscent of the density rotation predicted in elliptical double QDs,[21] where with interdot detuning, triplet energy levels E_T cross, while singlet energy levels E_S anticross, as dictated by the symmetry of the constituent single-particle states, in agreement with the von Neumann-Wigner theorem in molecular physics.[22] Therefore, the exchange energy $J(=E_T-E_S)$ exhibits a cusp in its dependence on detuning. For $V_T \gg V_L=V_R$ [Fig. 3(a), row(iv)], the electrons are effectively in a single QD as the potential energy of the top dot is much lower than that of the left and the right dots. Accordingly, the density plot [Fig. 3(a), row(iv)] shows both the singlet and the triplet electrons predominantly occupying the top dot. The exchange energy is largest in this region since triplet electrons occupy a higher-energy p orbital to form a sp pair due to the Pauli exclusion principle, whereas

singlet electrons remain for the most part on the low-energy s orbital. We observe that the triplet densities look more elliptical than the singlet densities because of the increased effective separation between parallel spins due to their exchange interactions.

In Fig. 3(b), we plot the exchange energies as functions of V_T for four different values of r_T (20, 25, 30, and 35 nm), while keeping V_L and V_R set at 25 meV and $r_L=r_R=30$ nm. At $V_T=0$ meV, all four exchange curves converge to a same energy value ($\sim$0.27 meV) since the model potential is independent of r_T at this bias [Eq. (2)]. For values close to $V_T=0$ meV, the exchange energy is relatively small for all r_T because the effective elimination of the top dot spatially decouples the two electrons into the left and the right QDs. For larger values of V_T, the exchange energy initially increases monotonically as the fraction of the total electron density occupying the top dot increases. Thus, the gates controlling the top-dot potential can be utilized to manipulate the system exchange energy. At values near $V_T=25$ meV, the potential depth of the three local minima are close to one another, resulting in a symmetric TQD system for $r_T=30$ nm and $V_T=25$ meV. We observe discontinuities in dJ/dV_T, which changes sign (from positive to negative) for all values of r_T, and is caused by the different localization of singlet and triplet electrons as mentioned above. For large (small) values of r_T, the depth of the top-dot potential well and the energy barrier between the top and the side dots decrease (increase), and as a result, the electron system effectively becomes a single dot (triple QD). Because the system coalesces into a single dot for larger values of r_T, a positive correlation between r_T and exchange energy is expected. Accordingly, we observe the J values at the cusp increase with r_T. We also notice the J cusp occurs at higher V_T for $r_T=35$ nm ($V_T=28.125$ meV) than for other values of r_T ($V_T=25$, 24.375, and 25 meV for $r_T=20$, 25, and 30 nm, respectively). This can be explained by noting that at larger r_T values, the top dot becomes shallower, inducing electron transfer from the side to the top dots at larger V_T values. For smaller r_T values, the confinement in the top dot is stronger; consequently the single-particle energy spacing increases. Since the dominant components of the triplet in a single QD are the sp_x and the sp_y orbitals,[14] larger differences between the s- and the p-orbital energy states results in higher triplet energies, leading to larger exchange energy for potentials with small r_T as illustrated in Fig. 3(b) for $V_T \approx 50$ meV.

Figure 4(a) shows the electron densities for $B=0$, 1, 2, and 3 T for the singlet ($V_T=25$ meV) and the triplet ($V_T=25$ and 25.625 meV) states. The singlet densities remain relatively unchanged with varying magnetic fields, while the abrupt change in the triplet charge-density configurations between $V_T=25$ and 25.265 meV is quenched by the presence of the magnetic fields that redistribute the density among the three dots. Here the magnetic field modifies the symmetry of the system by adding angular momentum in the electron motion. Specifically, upon applying magnetic fields, the p_x and the p_y parities mix forcing the electron wave functions to take a cylindrical symmetry.[21] As a result, the triplet density transition from the side QDs to the top dot evolves more smoothly with V_T.

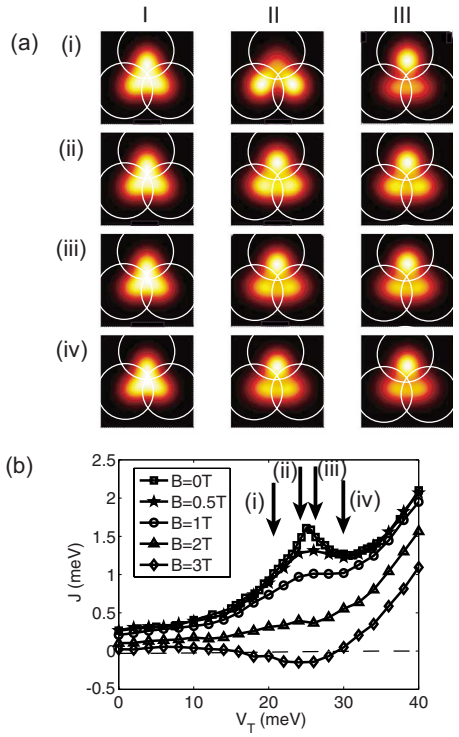

FIG. 4. (Color online) (a) Two-dimensional density plots for rows (i) $B=0$ T, (ii) $B=1$ T, (iii) $B=2$ T, and (iv) $B=3$ T. The circles indicate the location of the three dots. Columns I, II, and III correspond to the singlet density at $V_T=25$ meV, the triplet density at $V_T=25$ meV, and the triplet density at $V_T=25.625$ meV, respectively. (b) Exchange energy J as a function of V_T for magnetic field $B=0$, 0.5, 1, 2, and 3 T in a triangular TQD system. V_L and V_R are fixed at 25 meV and r_L, r_T, and r_R are set at 30 nm. The arrows correspond to density plots in Fig. 4(a) at four V_T values and the dotted line correspond to the Fermi-energy level. For $B=3$ T, the triplet becomes the lowest ground state when $J<0$ meV ($15.6<V_T<29$ meV). At the minimum, $J=-0.1482$ meV, which occurs at $V_T=24$ meV.

Figure 4(b) shows the dependence of the exchange energy on magnetic fields for $r_T=30$ nm in the detuning range corresponding to $0 \leq V_T \leq 40$ meV. Comparing the exchange-energy curves for $B=0$ and 0.5 T, the most notable differences are for $24 \leq V_T \leq 28$ meV, where the abrupt triplet density transition occurs at $B=0$ T. We see that at $B=1$ T, the J cusp evolves into an inflection point at around $V_T=26$ meV as a result of momentum redistribution caused by the magnetic field [Fig. 4(a)]. At $B=3$ T, a local minimum arises around $V_T=25$ meV: however, unlike for $B=0$ T, the behavior is the manifestation of a smooth transition in localization of both the singlet and the triplet electrons. Moving from $V_T=0$ to 40 meV at $B=3$ T, the ground state evolves from $S=0$ ($0 \leq V_T \leq 15.6$ meV) to $S=1$ ($15.6 \leq V_T \leq 29$ meV) to $S=0$ ($29 \leq V_T$ meV) states.

Next, we consider three quantum dots collinearly along a line.[7] The distances between the top and the left dots as well as the top and the right dots remain at 50 nm, while the distance between the left and the right dots doubles to 100 nm. All other parameters remain the same as in the triangular TQD. Figure 5(a) shows the singlet and the triple densities

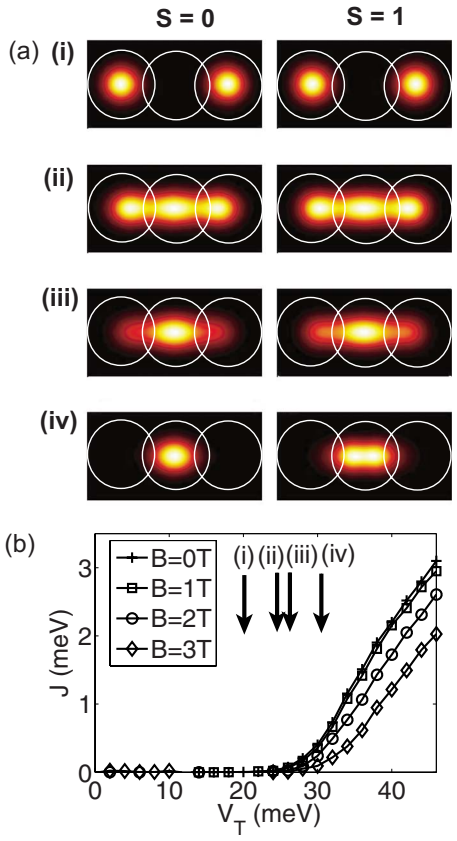

FIG. 5. (Color online) (a) Two-dimensional density plots in a collinear TQDs for $r_T=30$ nm. The circles indicate the location of the three dots. Rows (i), (ii), (iii), and (iv) correspond to $V_T=10$, 26, 30, and 40 meV, respectively. The first column (second column) shows the singlet (triplet) electron densities. Light (dark) color corresponds to high (low) density. (b) Exchange energy J as a function of V_T for magnetic field $B=0$, 0.5, 1, 2, and 3 T for a collinear TQDs. V_L and V_R are fixed at 25 meV and r_L, r_T, and r_R are set at 30 nm. The separation between the center-left and center-right QDs is 50 nm, while the separation between the left-right QDs is 100 nm. The arrows correspond to density plots in Fig. 5(a) at four V_T values.

for four different values of V_T (10, 26, 30, and 40 meV; here V_T is the potential in the central dot) for $B=0$ T. Density plots for nonzero magnetic fields are qualitatively similar due to gradual electron relocalization to the center QD. For $V_T<25$ meV, there are strong localizations in the left and right dots for both the singlet and the triplet densities [Fig. 5(a), rows (i) and (ii)]. Figure 5(b) shows the exchange-energy curves for $B=0$, 1, 2, and 3 T. The general behavior of the exchange curves for all four magnetic-field values is similar for all magnetic fields with the exchange energy being close to zero at smaller V_T and increasing quasilinearly for $V_T \geq 26$ meV. Comparison of exchange-energy values at $V_T=0$ meV (0.0023 meV for collinear TQD and 0.2671 meV for triangular TQD) reflects the different interdot separation values and charge densities. At $V_T=26$ meV, the two electrons are spread over all three dots, and as a result, the exchange energy increases [Fig. 5(b)]. For higher V_T, the electrons primarily occupy the central dot for both the singlet and the triplet [Fig. 5(a) row(iii)], while the densities evolve

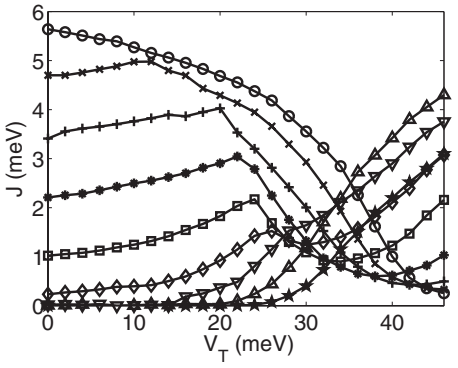

FIG. 6. J as a function of V_T (from 0 to 46 meV) for angles $=0$ ("o" symbol), 20° ("x" symbol), 30° ("+" symbol), 40° ("●" symbol), 50° ("■" symbol), 60° ("◇" symbol), 70° ("▽" symbol), 90° ("△" symbol), and 180° ("∗" symbol).

accordingly. Unlike in the triangular configuration, the dJ/dV_T for all values of V_T remains continuous in the collinear TQD [Fig. 5(b)]. Indeed the lowest excited state always remains the p_x state and as such, there is no symmetry change in the electronic states during the detuning change. So energy levels do not cross one another,[20] and as a result, no cusp in the J curves is observed.[21] Finally, at $V_T=40$ meV, electrons occupy only the central dot [Fig. 5(a) row(iv)]. As in the triangular TQD, we observe two maxima peaks for the triplet densities. These peaks are aligned along the coupling direction of the dots (x direction) due to the collinear alignment of the QDs along this direction and resulting ellipticity of the central QD (Ref. 19).

Next, we investigated the J dependence on the angle θ between the two segments connecting the centers of the top and left/right QDs. We vary the angle from 0 to 180° while keeping the distance between the top and the left/right QDs constant at $D=50$ nm. Effectively, the distance between the left and the right QD changes as a function of the angle. In Fig. 6, we plot the exchange-energy curves for TQD systems for different angles. At small angles and at $V_T=0$ meV, the left and the right dot overlap, forming a single circular dot that is twice as deep as the top dot. For small V_T, the two electrons predominantly localize in the deeper dot and, as a result, the exchange energy is large (~5 meV). For larger values of V_T, the exchange interaction decreases as electrons leak into the top dot, lowering the Coulomb energy. Due to the circular symmetry of the dot system, no charge-density rotation occurs,[21] and as a result, the exchange-energy curves are smooth. For $V_T>50$ meV, the top dot becomes deeper than the combination of left and right dots and thus, the exchange interaction increases again as the system become effectively a single dot (not shown in the figure). For larger angles, the left-right dot coupling becomes more elliptical as the aspect ratio increases with large angles.[21] Thus, for $\theta \sim 20°$, we observe the J cusp due to the density rotation. Because the aspect ratio of the coupled dots increases with larger angles, the Coulomb energy decreases and the transition to the top dot occurs later at larger V_T values. As a result, the V_T values corresponding to the cusp increase monotonically from 20 to 60°. At angles larger than 70°, the kink in J curves disappears again as TQDs approach collin-

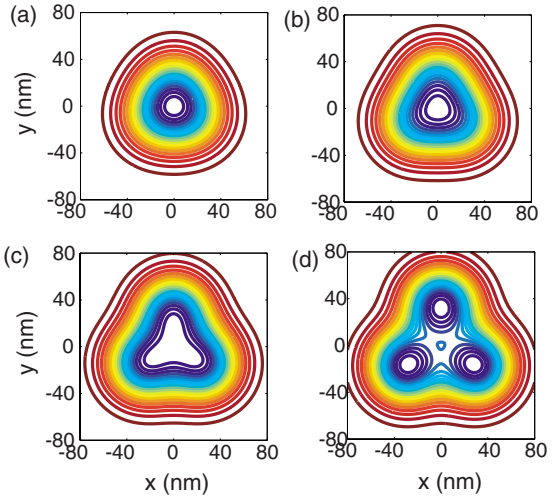

FIG. 7. (Color online) Two-dimensional potential contour plot for TQD with (a) $D=30$ nm, (b) $D=40$ nm, (c) $D=50$ nm, and (d) $D=60$ nm, where D represents the distance between the minima of the individual QDs (all the distances are equal since the TQD is set to be equilateral). The white space region near the $x=0$ and $y=0$ nm marks the location of the QDs except for $D=60$ nm case in which an energy barrier forms near the $x=0$ and $y=0$ nm point.

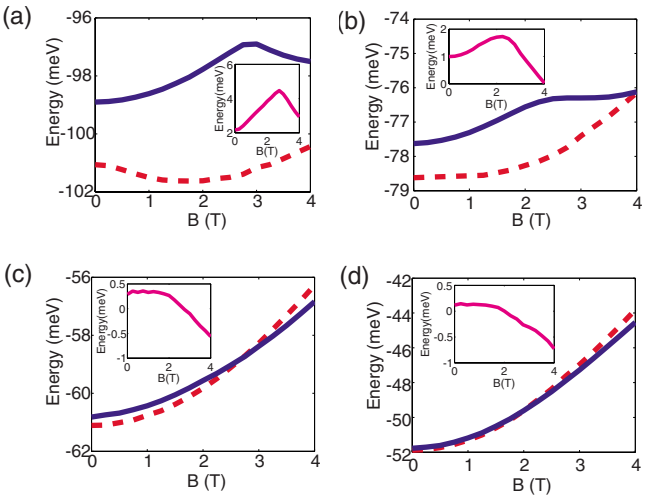

FIG. 8. (Color online) TQD total-energy (solid lines for $S=3/2$ and dashed lines for $S=1/2$) curves for $N=3$ electrons from $B=0$ to 4 T. (a) $D=30$ nm, (b) $D=40$ nm, (c) $D=50$ nm, and (d) $D=60$ nm. Inset shows Δ_{QD} curves. The small oscillations seen in Figs. 8(c) and 8(d) are of numerical origin in the Monte Carlo method.

ear geometries. Since the shapes of the QDs do not interfere with one another at larger angles, the qualitative behavior of the exchange curves is similar for all angles larger than 90°.

For $N=3$ electrons, we use four different interdot separation values: $D=30$, 40, 50, and 60 nm. The contour potential profile can be seen in Fig. 7, in which the location of the QDs is indicated by the confined white spaces near the center of the respective subplots. It is seen that the potential profile gradually changes from a single QD ($D=30,40$ nm) to a coupled ($D=50$ nm) and decoupled ($D=60$ nm) TQD for different values of D.

In Fig. 8, we plot the doublet ($S=1/2$) and the quadruplet ($S=3/2$) energies with their difference, ($\Delta_{QD}=3/2J$), in inset for the four different values of D (30, 40, 50, and 60 nm). For $D=30$ nm [Fig. 8(a)], the behavior of the curves look very much alike in the single QD case, which is expected since the potential profile is similar to a circular single QD [Fig. 7(a)]. The exchange energy among electrons is relatively high accordingly, due to the close physical proximity of the electrons. For $D=40$ nm [Fig. 8(b)], the system is still a single QD, but its shape is more triangular [Fig. 7(b)]. In Fig. 8(b), we observe the change of the kink in the quadruplet ($S=3/2$) energy curve into an inflection point at $B\approx 2.5$ T. Also, the doublet ($S=1/2$) energy now increases monotonically with the magnetic field, unlike the behavior observed in the $D=30$ nm case. Accordingly, the exchange energy becomes smoother near the local maximum point at $B\approx 2$ T. At around $B=4$ T, the system undergoes a doublet-quadruplet transition with the $S=3/2$ becoming the ground state (similar to the ones found for $N=2$ electrons between the singlet and triplet states). For $D=50$ and 60 nm [Figs. 8(c) and 8(d)], the three dots become more distinctive. Both the doublet and the quadruplet energies increase monotonically versus magnetic fields, and as a result, the local maximum in the exchange energy disappears. However, the doublet-quadruplet transition occurs at lower magnetic fields ($B=2.7$ T for $D=50$ nm and $B=2.0$ T for $D=60$ nm, respectively), while the exchange energy at $B=0$ T decreases as D increases. For the coupled TQD [Fig. 8(c)], the Δ_{QD} value at $B=0$ T is 0.289 meV while for the decoupled TQD [Fig. 8(d)], it is 0.1168 meV. The higher Δ_{QD} value at $B=0$ T for the coupled QD case is expected due to the closer proximity of the dots, leading to greater sp-orbital occupation for the $S=3/2$ state. As mentioned in Sec. I, the ground state for zero magnetic field is always the $S=1/2$ state resulting in $J>0$ for all device parameters. Oscillating behaviors found in the exchange energy at low magnetic fields are due to numerical fluctuations in the Monte Carlo method.

Figure 9(a) displays the two-dimensional plot of the quadruplet-doublet energy difference Δ_{QD} with respect to D and magnetic fields. Upon evolving from single to triple QD with increasing D in the investigated magnetic-field range (from $B=0$ to 4 T), Δ_{QD} decreases in magnitude and the kink at $B\approx 2.7$ T develops into a smooth maximum to finally disappear at large D. One also observes the onset of the doublet-quadruplet transitions that for increasing $D=40$, 45, 50, 55, and 60 nm moves from 4, 3.27, 2.7, 2.29, and 2 T. In Fig. 9(b) we show the spin phase diagram as a function of B and D. It is seen that with the decoupling of the QDs, the magnetic field at the transition is less sensitive to the distance separating the QDs.

Next, we investigate the effect of electrical detuning on the $N=3$ TQD system. Specifically, we vary one of the gate biases (V_T in this case) and analyze its effect on Δ_{QD}. We plot Δ_{QD} as function of V_T for both $D=50$ nm (i.e., coupled) and $D=60$ nm (i.e., decoupled) TQDs in Fig. 10(a), while keeping other parameters in the model potential constant ($V_L=V_R=25$ meV and $r_L=r_T=r_R=30$ nm). For $V_T<12$ meV, the electrons occupy the left and the right QDs, leaving the top QD vacant. Accordingly, Δ_{QD} is insensitive to changes in V_T in this detuning range, which is reflected by

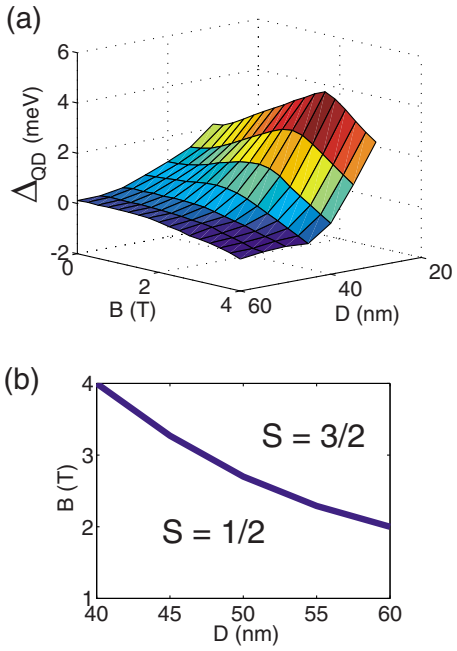

FIG. 9. (Color online) (a) Two-dimensional exchange curve as a function of D and magnetic fields. From single-QD ($D=20$ nm) to triple-QD ($D=60$ nm) configuration, the Δ_{QD} values decrease in magnitude, local maxima ceases to exist, and the curve crosses zero somewhere in this magnetic-field regime. (b) The solid line indicates the doublet-quadruplet transition; above this line, the ground state is $S=3/2$, while below this line the ground state is $S=1/2$. The dotted line is a linear segment connecting the two points ($B=4$ T and $D=40$ nm; $B=1$ T and $D=60$ nm) and it serves as a guidance on the shape of the solid line. The contour potential plots (for $D=40$ and 60 nm are included in the inset as a guidance on the shape of the TQD system.

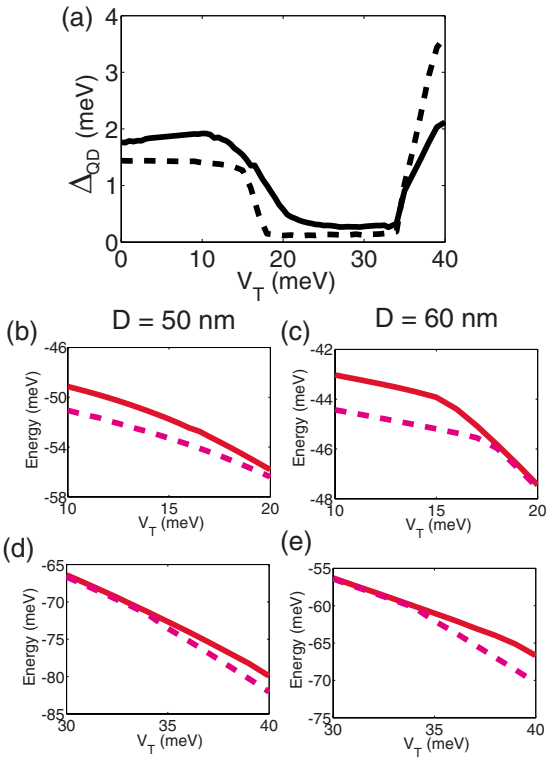

FIG. 10. (Color online) (a) Δ_{QD} as a function of V_T (from 0 to 40 meV). The two TQD systems are $D=50$ (solid line) and 60 nm (dashed line). The $S=1/2$ and $S=3/2$ (b) at $D=50$ nm with V_T from 10 to 20 meV, (c) at $D=60$ nm with V_T from 10 to 20 meV, (d) at $D=50$ nm with V_T from 30 to 40 meV, and (e) at $D=60$ nm with V_T from 30 to 40 meV. For each of the figures [(b)–(e)], the solid line represents the $S=3/2$ states and the dashed lines represent the $S=1/2$ states.

the flatness of the two curves ($D=50$ and 60 nm). For $D=50$ nm, the three dots are more coupled compared to the $D=60$ nm case, which increases the sensitivity of Δ_{QD} for $V_T<12$ meV. At $V_T\geq 12$ meV, Δ_{QD} abruptly drops as one of the electrons moves into the initially empty top dot and the system lowers its energy to reach equilibrium with one electron per dot. Accordingly, the electrons predominantly occupy the single-particle s-orbital states in the three respective dots, and as a result, the energy difference between the doublet and the quadruplet becomes relatively small compared to the three electrons in the double-dot configuration. In the limiting case of $D\rightarrow\infty$, the $S=1/2$ and $S=3/2$ energies become equal. In Figs. 10(b) and 10(c), we plot the total energies of the $S=3/2$ and $S=1/2$. As we can see, more noticeable for $D=60$ nm [Fig. 10(c)], the slope of the $S=3/2$ curve is steeper at smaller V_T values compared to the $S=1/2$ curve, with the change in slope indicating electron relocalization. This can be explained by the Pauli exclusion principle since the parallel spins in the $S=3/2$ state entails that electrons would spread themselves out over a wider region. With an electron now occupying the top QD, the absolute value of the ($S=3/2$) slope increases (from 0.1378 to 0.885 meV/V at $V_T=15.5$ meV) as V_T exerts more influence on the total system energy due to the physical proximity of the top gate to the electron. For $D=50$ nm, the Δ_{QD} curve is smoother than for $D=60$ nm in the transition region ($12<V_T<20$ meV) because of the overall coupling between the QDs, which prevents abrupt density transitions as discussed in the double QD case.[21] Also, even when the system configures itself to one electron per QD ($22<V_T<32$ meV), Δ_{QD} is still higher for the $D=50$ nm TQD because of closer physical proximity among electrons.

Around $V_T\approx 32$ meV, there is another abrupt transition in Δ_{QD}, which is caused by the relocalization of the second electron into the top QD. We plot the total energies of the $S=3/2$ to 1/2 states in Figs. 10(d) and 10(e); in this case the $S=1/2$ slope is steeper at smaller V_T values than the $S=3/2$ curve. Again this is attributed to the Pauli exclusion principle: the double occupancy of the top QD for antiparallel electrons (corresponding to the $S=1/2$ configuration) becomes more favorable than for parallel electrons (corresponding to the $S=3/2$ configuration). For $D=60$ nm, the Δ_{QD} slope changes from 0.885 to 1.696 meV/V around $V_T=32$ meV and accordingly the change in the exchange interaction is greater here than at $V_T=16$ meV. After this transition, the third electron spreads equally across the left and the right QDs. For higher V_T, the top QD eventually is triply occupied as in a single QD system.

In Fig. 11, we display the chemical potentials of the TQD structure at $D=50$ nm, $\mu(N)=E_T(N)-E_T(N-1)$, where N is

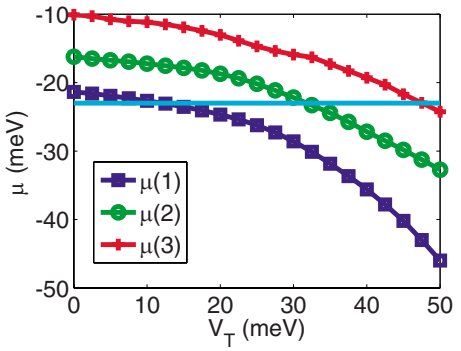

FIG. 11. (Color online) Chemical potential $\mu(N)$ as a function of V_T for $N=1$, 2, and 3. The horizontal line (=−22.5 meV) indicates the reference chemical-potential value for the drain/source regions of the QDs.

the number of electrons in the system for $N=1$, 2, and 3 as a function of V_T. The chemical potentials were computed using the data for $N=2$ electrons and $N=3$ electrons as well as a new set of simulation results for $N=1$ electrons [note that $E_T(0)\equiv 0$]. There is a monotonic decrease in chemical potentials with respect to detuning voltage V_T as separation between $E_T(N)$ and $E_T(N-1)$ increases for all N, as the TQD approaches the single dot configuration. In order to find the addition energy, we choose a constant reference value for the chemical potential of −22.5 meV in the source/drain of the QD device. At this value, the chemical potential in the source/drain region is just above the minima of the model potential along the left and the right QDs (−25 meV). From the figure, we can calculate the additional energy by taking the difference in the V_T values where the chemical-potential curves cross the horizontal-reference curve. The first two additional energies are computed to be around 22 and 16 meV.

V. SUMMARY

We have shown the electrical tunability of exchange energies and charge densities for two and three electrons in both the triangular and collinear TQD systems using the variational Monte Carlo method. We observed a nonmonotonic variation in the exchange energy J, which is characterized by a discontinuity in the dJ/dV_T as a function of the detuning voltage in QDs with triangular configurations. This phenomenon is attributed to the abrupt relocalization of the triplet density in the top QD, which persists as long as the top angle of the QD isosceles triangle varies between ~20° and ~70°. Unlike the double QD system, the presence of the third dot provides another degree of freedom that allows the cusp to manifest itself without directly disturbing the other two QDs. We have also shown that this effect is quenched by the presence of a perpendicular magnetic field that smoothes out the triplet transition from the side dots to the top dot under detuning. For three electrons, nonmonotonic variation in exchange energy persists in low magnetic-field regime in coupled triangular TQDs, but not in the more decoupled triangular TQDs. In detuned triangular TQDs, the quadruplet and doublet states localize at different V_T values, causing an abrupt change in the difference between the two ground states. Finally, the addition energy in the triangular TQD system is calculated by fixing the drain/source chemical potential at a reference value just above the potential minima of the symmetric TQD system.

ACKNOWLEDGMENTS

We are grateful to R. M. Martin and M. Casula for helpful discussion. This work was supported by the Material Computational Center. The work performed at the Materials Computation Center was supported by the National Science Foundation under Grant No. DMR-03 25939 ITR, with additional support through the Frederick Seitz Materials Research Laboratory (U.S. Department of Energy under Grant No. DEFG02-91ER45439) at the University of Illinois Urbana-Champaign. Parts of the simulations were conducted using the Turing Cluster, which is operated by the School of Computational Science and Engineering.

[1] L. P. Kouwenhoven, C. M. Markus, P. L. McEuen, S. Tarucha, R. M. Westervelt, and N. S. Wingreen, in *Mesoscopic Electron Transport*, edited by L. L. Sohn, L. P. Kouwenhoven, and G. Schön, NATO Advanced Study Institute, Series E Vol. 345 (Kluwer, Dordrecht, 1997), p. 105.

[2] W. G. van der Wiel, S. D. Franceschi, J. M. Elzerman, T. Fujisawa, S. Tarucha, and L. P. Kouwenhoven, Rev. Mod. Phys. **75**, 1 (2002).

[3] S. Tarucha, D. G. Austing, T. Honda, R. J. van der Hage, and L. P. Kouwenhoven, Phys. Rev. Lett. **77**, 3613 (1996).

[4] A. W. Holleitner, R. H. Blick, A. K. Huttel, K. Eberl, and J. P. Kotthaus, Science **297**, 70 (2002).

[5] F. H. Koppens, J. A. Folk, J. M. Elzerman, R. Hanson, L. H. W. van Beveren, I. T. Vink, H. P. Tranitz, W. Wegscheider, L. P. Kouwenhoven, and L. M. K. Vandersypen, Science **309**, 1346 (2005).

[6] J. R. Petta, A. C. Johnson, J. M. Taylor, E. A. Laird, A. Yacoby, M. D. Lukin, C. M. Marcus, M. P. Hanson, and A. C. Gossard, Science **309**, 2180 (2005).

[7] J. Kim, D. V. Melnikov, J. P. Leburton, D. G. Austing, and S. Tarucha, Phys. Rev. B **74**, 035307 (2006).

[8] D. S. Saraga and D. Loss, Phys. Rev. Lett. **90**, 166803 (2003).

[9] A. Vidan, R. M. Westervelt, M. Stopa, M. Hanson, and A. C. Gossard, Appl. Phys. Lett. **85**, 3602 (2004).

[10] M. Stopa, Phys. Rev. Lett. **88**, 146802 (2002).

[11] C. S. Lent, P. D. Tougaw, W. Porod, and G. H. Bernetin, Nanotechnology **4**, 49 (1993).

[12] D. Schroer, A. D. Greentree, L. Gaudreau, K. Eberl, L. C. L. Hollenberg, J. P. Kotthaus, and S. Ludwig, Phys. Rev. B **76**, 075306 (2007).

[13] M. Korkusinski, I. P. Gimenez, P. Hawrylak, L. Gaudreau, S. A. Studenikin, and A. S. Sachrajda, Phys. Rev. B **75**, 115301

(2007).
[14] J. Kim, D. Melnikov, and J. P. Leburton, Open Condens. Matter Phys. J. **1**, 1 (2008).
[15] I. Puerto Gimenez, M. Korkusinski, and P. Hawrylak, Phys. Rev. B **76**, 075336 (2007).
[16] D. V. Melnikov, J. P. Leburton, A. Taha, and N. Sobh, Phys. Rev. B **74**, 041309(R) (2006).
[17] W. L. McMillan, Phys. Rev. **138**, A442 (1965).
[18] D. M. Ceperley and B. J. Alder, Phys. Rev. B **16**, 3081 (1977).
[19] H. Saarikoski, E. Rasanen, S. Siljamaki, A. Harju, M. J. Puska, and R. M. Nieminen, Eur. Phys. J. B **26**, 241 (2002).
[20] V. Fock, Z. Phys. **47**, 446 (1928).
[21] L.-X. Zhang, D. V. Melnikov, and J. P. Leburton, Phys. Rev. B **78**, 085310 (2008).
[22] J. von Neumann and E. Wigner, Z. Phys. **30**, 467 (1929); L. D. Landau and E. Lifshitz, *Quantum Mechanics: Non-Relativistic Theory* (Pergamon, Oxford, 1977).